Neutron Star Mass Distributions and the Equation of State of Dense Matter

Mahmudul Hasan Anik[1,*] and Andrew W. Steiner[1,2]

[1] *Department of Physics and Astronomy, University of Tennessee at Knoxville, Tennessee 37996, USA*
[2] *Physics Division, Oak Ridge National Laboratory, Tennessee 37830, USA*

We combine neutron star (NS) mass measurements with electromagnetic and gravitational wave observations to construct a comprehensive model which can describe the mass distributions of neutron stars in binaries and the dense matter equation of state (EoS). To understand how the mass distributions vary by populations, we assign different models to NS binaries depending on the companion stars: NS-NS or double neutron stars (DNS), NS – white dwarfs (NS-WD), and low-mass X-ray binaries (LMXBs). In addition, we include two EoS models and study how different choices of the EoS impact the constraints on the NS mass-radius curve. Finally, we study how prior assumptions on the maximum mass create uncertainties in the nature of observable matter at the high densities. Our current results show that NS masses in DNS, NS-WD, and LMXB have distinct probability densities with the peaks at 1.4 $M_\odot$, 1.6 $M_\odot$, and 1.7 $M_\odot$, respectively. We also observe that the softness of the EoS differs between our two EoS models and thus depends on the prior choice.

I. INTRODUCTION

Neutron star observations provide insight to the strong interactions of dense matter under extreme conditions. Studying the EoS and the underlying NS mass-radius relation has become a primary focus of nuclear physics and astrophysics since the discovery of neutron stars in 1967. In this era of multi-messenger astronomy, an increasingly growing number of observational data from various sources are becoming available. This includes mass-radius measurements from observations of globular clusters [1], type-I X-ray bursters [2], NICER X-ray timing observations [3, 4], mass measurements from radio timing of pulsars [5–7], and the LIGO-Virgo observations of gravitational waves (GWs) [8, 9]. Hence, a comprehensive model describing these data sets is key to understanding the NS structure and can shed light on further constraints of the EoS and the mass-radius curve.

Combining electromagnetic (EM) mass-radius data and LIGO observation of GW170817 [8] established the best constraints on the NS mass-radius curve to date [10]. The EM data included observations of Quiescent Low-Mass X-ray Binaries (QLMXBs), Photospheric Radius Expansion X-ray bursters (PREs), and the NICER observation of the isolated pulsar PSR J0030+0451. However, this study included only NS mass-radius relations based on different EoS models and no mass distribution models. On the other hand, recent works extensively studying the NS mass distribution models (see e.g. Refs. [5–7]) focused on mass measurements with no radius or EoS information. These works study different mass distributions based on the NS companion types (in binaries), the stellar evolution stages, or the detection methods. On the contrary, Ref. [8] considers only mass distributions that fit the observations and presumes that all NS populations have the same distribution. No model has been constructed to combine the NS mass distributions, the EM mass-radius distributions, and the GW observations to obtain a complete picture of strong interactions in dense matter.

Our approach to this problem is to classify NS in binaries by the companion stars for which the NS masses have been observed. We model the mass distributions for each population and incorporate the mass-radius distribution with our dense matter EoS models and the GW observations. Thus, we obtain a combined probability distribution of NS masses and the EoS. We also explore how different choices of EoS models with different parametrizations impact the uncertainties on the NS mass-radius relation. Finally, we study how the results change when the NS maximum mass is considered as a parameter with a prior distribution.

In the next section, we discuss our theoretical models for the NS mass distribution, the dense matter EoS, and the GW observations. Then in Section III, we provide an overview of Bayesian inference and our parameters and prior choices. Next in Section IV, we present our current results (work in progress) and compare with recent works. Finally, we briefly describe our future goals in Section V.

II. THEORETICAL FRAMEWORK

An equation of state (EoS) is a thermodynamic relationship between state variables such as pressure, temperature, and internal energy. The EoS is usually expressed as the pressure P as a function of the energy density ϵ. For a given EoS of neutron stars and the boundary conditions, the Tolman–Oppenheimer–Volkoff (TOV) equation from general relativity provides a unique NS mass-radius relation. The TOV equations are a set of coupled first-order ordinary differential equations which, for a static and spherically symmetric star, takes the

* anik@vols.utk.edu

form:

$$\frac{dP}{dr} = -\frac{G\epsilon m}{r^2}\left(1+\frac{P}{\epsilon}\right)\left(1+\frac{4\pi P r^3}{m}\right)\left(1-\frac{2Gm}{r}\right)^{-1} \tag{1}$$

where r is the radial coordinate, $m(r)$ is the gravitational mass enclosed within a radius r, $\epsilon(r)$ and $P(r)$ are the energy density and the pressure at r, and G is the Gravitational constant. The enclosed mass is related to the energy density by

$$\frac{dm}{dr} = 4\pi r^2 \epsilon. \tag{2}$$

In the above equations, we used natural units: $\hbar = c = 1$, where $\hbar$ is the reduced Planck constant and c is the speed of light. The above two differential equations can be solved simultaneously given an EoS in the form $P(\epsilon)$, the initial value of the central pressure $P(r=0) = P_c$, and the boundary conditions:

$$m(r=0) = 0, \qquad P(r=R) = 0,$$

where R is the radius. Then the total gravitational mass $M(r=R)$ can be computed by evaluating the integral

$$M = \int_0^R 4\pi r^2 \epsilon(r)\, dr. \tag{3}$$

Thus, each value of the central pressure P_c implies a point (M, R) and thus defines a mass-radius $(M-R)$ curve for a given set of values of P_c.

We work with EoS models at densities observed in neutron stars, where matter is degenerate and consists only of neutrons, protons, and electrons. In this regime, $\mu \gg T$, where μ is the chemical potential and T is the temperature. Thus, in the $T = 0$ approximation, our dense matter EoS (in unit volume) has the form:

$$P + \epsilon = n_n\mu_n + n_p\mu_p + n_e\mu_e, \tag{4}$$

where ϵ is the internal energy density, P is the pressure, n_i is the number density, and μ_i is the chemical potential of the particle i. Assuming charge neutrality $n_p = n_e$, and beta equilibrium $\mu_n = \mu_p + \mu_e$, the above identity reduces to

$$P + \epsilon = n_b\mu_b, \tag{5}$$

where $n_b = n_n + n_p$ is the baryon number density and $\mu_b \equiv \mu_n$ is the baryon chemical potential. Thus in this simple model, we assume that the thermodynamic properties of neutron star matter behave as if matter consists of a single component. Given a set of points (ϵ, n_b), we can compute μ_b and P using the above relationship:

$$\mu_b = \frac{\partial \epsilon}{\partial n_b}, \qquad P = n_b^2\,\frac{\partial(\epsilon/n_b)}{\partial n_b}. \tag{6}$$

The relative speed of sound squared is defined as

$$c_s^2 = c^2\left(\frac{\partial P}{\partial \epsilon}\right)_x, \tag{7}$$

where x indicates a fixed ratio between the neutron, proton, and electron densities. In the natural unit ($c = 1$), $c_s^2/c^2 \equiv c_s^2 < 1$.

A. NS Mass Model

In this study, neutron stars are assumed to be non-rotating, isotropic, and spherically symmetric. We also assume that the NS mass distributions differ by populations, but remain unchanged for each population. More succinctly, the individual neutron stars may undergo stellar evolution, but their overall mass distribution in a given population is fixed and independent of time.

For each NS which has a mass observation (indexed by i), there is an observed mass, m_i which may differ from the actual mass of the NS, M_i. We define w_i to be the difference of these two

$$m_i = M_i + w_i, \quad i = 1, \ldots, n \tag{8}$$

1. Mass Distribution

We assume that the neutron star mass distributions are skewed normal distributions, and that the values of M_i, are selected from that distribution. The skewed normal NS mass distribution is given by

$$\mathrm{SN}(M \,|\, \mu, \sigma, \alpha) = \frac{2}{\sigma}\,\phi\Big(\frac{M-\mu}{\sigma}\Big)\,\Phi\Big[\frac{(M-\mu)\alpha}{\sigma}\Big], \tag{9}$$

where ϕ is the standard normal distribution functions, $N(0,1)$, and Φ is the associated cumulative distribution function. Here, $\mu \in \mathbb{R}$, $\sigma \in \mathbb{R}^+$, and $\alpha \in \mathbb{R}$ are location, scale, and skewness parameters, respectively. Note that setting $\alpha = 0$ yields the normal distribution $N(\mu, \sigma)$, while $\alpha > 0$ gives right-skewness and $\alpha < 0$ results into left-skewness. Thus, this choice of distribution enables us to study a wide variety of mass distributions in different NS populations.

2. Uncertainty Distribution

The mass uncertainty data for the populations of DNS and NS-WD contain asymmetry in some of the 68% error bars of the mass estimates. That is, for some mass estimates $m_i \in [m_i - l_i,\, m_i + u_i]$, we have $l_i \neq u_i$, especially in the DNS population. In addition, similar to the mass distribution model, we still require that the uncertainty distribution reduces to a normal distribution as a special case. Hence, we assume w_i is drawn from an asymmetric normal distribution given by

$$\mathrm{AN}(w \,|\, c, d) = \frac{2}{d\big(c + 1/c\big)}\,\Big[\phi\Big(\frac{w}{cd}\Big)\,\chi_{[0,\infty)}(w) + \phi\Big(\frac{cw}{d}\Big)\,\chi_{(-\infty,0)}(w)\Big], \tag{10}$$

where $c \in \mathbb{R}^+$ is an asymmetry parameter, $d \in \mathbb{R}^+$ is a scale parameter, and $\chi_A(x)$ is the indicator function of the set A that returns 1 if $x \in A$ and 0 otherwise. Note

that for $c = 1$, Eq. (10) reduces to a normal distribution $N(0, d)$. For $c > 1$, the distribution is right-skewed and for $c < 1$, it is left-skewed. The parameters (c_i, d_i) for the ith star can be calculated from the 68% limits (l_i, u_i) in the data. The value c_i is determined by $c_i = \sqrt{u_i/l_i}$. Then for a given c_i, we solve for d_i such that

$$\int_{-l}^{u} \mathrm{AN}(x|c, d)\, dx = 0.68\,. \tag{11}$$

Note that $c = 1$ in the case of symmetric error bars since $l_i = u_i$, which results into the normal distribution $N(0, d)$. The details of these calculations are given in Appendix A.

3. Maximum Mass Cutoff

In order to prevent assigning a non-zero likelihood for the NS masses larger than the maximum mass, we introduce a Heaviside step function to the likelihood:

$$\Theta(M_{\max} - M_{i,j}) = \begin{cases} 1, & \text{if } M_{i,j} < M_{\max} \\ 0, & \text{otherwise} \end{cases} \tag{12}$$

Since we have no knowledge of the maximum mass for each population, it is reasonable to examine the likelihood of a global maximum mass for all populations.

Note that the NS mass M is often expressed as the mass fraction, which is related to the maximum mass by

$$m_{\mathrm{f}} = \frac{M - 1}{M_{\max} - 1}, \tag{13}$$

where $0 < m_{\mathrm{f}} < 1$.

B. EoS Models

Our EoS is the pressure $P(\epsilon)$ as a function of the energy density, often computed as a function of the baryon number density $P(n_b)$. For densities up to $2n_0$, where $n_0 = 0.16$ fm^{-3} is the nuclear saturation density, we assume that matter is dominated by neutrons and use the EoS from Gandolfi *et al.* [11] for pure neutron matter. We refer to this model as the "low-density EoS", which is constructed based on 2- and 3-nucleon interactions using quantum Monte Carlo (QMC) techniques. Above densities $n_b > 2n_0$, we make no such assumptions since we have no information regarding the composition of matter in higher densities. In this regime, we use either a polytropic or a linear EoS. The polytropic model consists of three piecewise polytropes and the linear EoS consists of three piecewise line segments. Both models are continues and differentiable everywhere except at the transitions between polytropes (or line segments) respectively. Furthermore, the EoS models do not include any nuclear interactions (or exchanges of mesons or any exotic matters) at higher densities since the degrees of freedom relevant to such densities are unknown. While both of our EoS models imply first order phase transitions, for the prior probability distributions which we give below, the linear EoS has a higher probability for strong phase transitions as compared to the polytropic EoS.

1. Low-Density EoS

We use the EoS model from Ref. [11] up to the baryon density $n_b = 2n_0$ (where $n_0 = 0.16$ fm^{-3} is the saturation density), which is expressed as a function of the baryon density

$$\epsilon(n_b) = a\left(\frac{n_b}{n_0}\right)^{\alpha} + b\left(\frac{n_b}{n_0}\right)^{\beta}. \tag{14}$$

Then the pressure is given by

$$P(n_b) = n_b\left[a\alpha\left(\frac{n_b}{n_0}\right)^{\alpha} + b\beta\left(\frac{n_b}{n_0}\right)^{\beta}\right], \tag{15}$$

where the parameters a, α, b, β are related to the symmetry energy S and its derivative L by

$$S = a + b + 16.0, \quad L = 3(a\alpha + b\beta). \tag{16}$$

The symmetry energy and its derivative are correlated, and thus further constrained [12] by,

$$(9.17S - 266.0\ \mathrm{MeV}) < L < (14.3S - 379.0\ \mathrm{MeV}) \tag{17}$$

Beyond $2n_0$, the EoS is constructed based on two methods: polytropic and linear.

2. Polytropic EoS

We refer to this EoS model as NP in our work, which is a 3-polytropic EoS of the form:

$$P(\epsilon) = K\epsilon^{1+1/n} = K\epsilon^{\gamma}, \tag{18}$$

where K is a proportionality constant, n is the polytropic index, γ is the adiabatic index, which are related by

$$n = \frac{1}{\gamma - 1}. \tag{19}$$

As explained above, we use the low-density EoS up to the baryon density $n_{b,1} = 2n_0$, when we calculate the energy density $\epsilon_1 = \epsilon(n_{b,1})$ and the pressure $P_1 = P(n_{b,1})$.

For the first polytrope, we compute the coefficient $K = P_1/\epsilon_1^{\gamma}$. Then, beginning at $(\epsilon_1, n_{b,1}, P_1)$, the baryon density along the polytrope is

$$n_b = n_{b,1}\left(\frac{\epsilon}{\epsilon_1}\right)^{\gamma/(\gamma-1)}\left(\frac{\epsilon_1 + P_1}{\epsilon + P}\right)^{1/(\gamma-1)}, \tag{20}$$

which can be used to compute the energy density

$$\epsilon(n_b) = \left[\left(\frac{n_{b,1}}{n_b\epsilon_1}\right)^{\gamma-1}\left(1+\frac{P_1}{\epsilon_1}\right) - K\right]^{-n}. \quad (21)$$

The pressure is then simply given by Eq. (18). Thus, the first polytrope is computed up to some transition density $\epsilon = E_1$. For the second polytrope, the above calculations are repeated until $\epsilon = E_2$, where $E_2 > E_1$, and similarly the third polytrope up to $\epsilon = 10.5$ fm^{-4}.

3. *Linear EoS*

The linear EoS, referred to as NL, consists of 3 line segments on the $P-\epsilon$ plane and assumes a fixed speed of sound c_s and a fixed energy density at zero pressure ϵ_0. The EoS has the form:

$$P(\epsilon) = c_s^2(\epsilon - \epsilon_0), \quad (22)$$

where c_s^2 is the relative speed of sound squared defined as $c_s^2 \equiv dP/d\epsilon$. Similarly as the polytropic EoS, we use the low-density EoS up to the baryon density $n_{b,1} = 2n_0$, the energy density $\epsilon_1 = \epsilon(n_{b,1})$, and the pressure $P_1 = P(n_{b,1})$.

Then to construct the first line segment, we use Eq. (22) to compute

$$\epsilon_0 = \epsilon_1 - \frac{P_1}{c_s^2}. \quad (23)$$

Beginning at $(\epsilon_1, n_{b,1}, P_1)$, the baryon density is given by

$$n_b = n_{b,1}\left[\frac{\epsilon(1+c_s^2) - c_s^2\epsilon_0}{\epsilon_1(1+c_s^2) - c_s^2\epsilon_0}\right]^{1/(1+c_s^2)} \quad (24)$$

$$= n_{b,1}\left(\frac{\epsilon+P}{\epsilon_1+P_1}\right)^{1/(1+c_s^2)}. \quad (25)$$

From the equation above, the energy density can be expressed as

$$\epsilon(n_b) = \frac{c_s^2\epsilon_0}{1+c_s^2} + \left(\frac{\epsilon_1+P_1}{1+c_s^2}\right)\left(\frac{n_b}{n_{b,1}}\right)^{1+c_s^2}, \quad (26)$$

and then the pressure is

$$P(n_b) = c_s^2\left(\epsilon_1 - \frac{c_s^2\epsilon_0}{1+c_s^2}\right)\left(\frac{n_b}{n_{b,1}}\right)^{1+c_s^2} - \frac{c_s^2\epsilon_0}{1+c_s^2}. \quad (27)$$

At some transition density $\epsilon = E_1$, the second line is computed using the above equations until $\epsilon = E_2$, where $E_2 > E_1$, and similarly the third line up to $\epsilon = 10.5$ fm^{-4}.

C. Gravitational-Wave Models

The gravitational wave observations GW170817 and GW190425 are both DNS, but are analyzed differently due to the nature of the measured quantities in the data sets. As explained in the Subsec. III A, the GW170817 observation measures the chirp mass in the detector frame ($\mathcal{M}_{\rm det}$), the mass ratio (q), and the redshift ($z_{\rm cdf}$).

Given ($\mathcal{M}_{\rm det}, q, z_{\rm cdf}$), the redshift z is computed from the inverse cumulative distribution of a Gaussian with a fixed mean 0.0099 and width 0.0009. Then the chirp mass is then given by

$$\mathcal{M}_{\rm chirp} = \frac{\mathcal{M}_{\rm det}}{1+z}, \quad (28)$$

from which the NS masses can be computed as follows:

$$M_1 = \frac{\mathcal{M}_{\rm chirp}(1+q)^{1/5}}{q^{3/5}} \quad (29)$$

$$M_2 = \mathcal{M}_{\rm chirp}\, q^{2/5}(1+q)^{1/5}. \quad (30)$$

Here, the mass ratio is defined as $q \equiv M_2/M_1$, where $M_1 > M_2$ so that $0 < q < 1$.

In the GW190425 observation, the chirp mass ($\mathcal{M}_{\rm chirp}$) is measured with high accuracy. We assume $\mathcal{M}_{\rm chirp}$ to be a constant and use it to find the mass M_2 given M_1 using the above equations. First, given the mass M_1, we define the constant

$$\frac{1+q}{q^3} = \left(\frac{M_1}{\mathcal{M}_{\rm chirp}}\right)^5 \equiv k. \quad (31)$$

Then we solve the cubic equation for q:

$$kq^3 - q - 1 = 0, \quad (32)$$

and compute M_2 from q.

III. BAYESIAN ANALYSIS

We employ Bayesian inference to determine credible intervals for our model parameters using the observational data. Bayes's theorem states that the posterior distribution of parameter θ given data d is (see Appendix C)

$$\mathcal{L}(\theta|d) \propto C\mathcal{L}(d|\theta)\ \pi(\theta), \quad (33)$$

where $\mathcal{L}(d|\theta)$ is the likelihood of the observation d given the parameter θ, $\pi(\theta)$ is the prior distribution of θ, and C is the normalization constant.

For a large number of parameters, computing the posteriors involves repeatedly evaluating high-dimensional integrals, which is computationally expensive. For this purpose, we use a C++ code `BAMR` that can effectively compute such integrals with high speed and accuracy using an algorithm called Markov Chain Monte Carlo (MCMC).

TABLE I. Stars in DNS with mass data and GW observations with probability distributions (denoted as $\mathcal{P}$). The symbol 'c.' next to a star name indicates the companion. Numbers following '±' are the ±68% central limits, and the ones next to '+' or '−' signs are the asymmetric 68% limits.

Star	Data (mass in $M_\odot$)	Reference
J0453+1559	1.559 ± 0.004	[7]
J0453+1559 c.	1.174 ± 0.004	[7]
J1906+0746	1.291 ± 0.011	[7]
J1906+0746 c.	1.322 ± 0.011	[7]
B1534+12	1.3332 ± 0.001	[7]
B1534+12 c.	1.3452 ± 0.001	[7]
B1913+16	1.4398 ± 0.0002	[7]
B1913+16 c.	1.3886 ± 0.0002	[7]
B2127+11C	1.358 ± 0.01	[7]
B2127+11C c.	1.354 ± 0.01	[7]
J0737-3039A	1.3381 ± 0.0007	[7]
J0737-3039B	1.2489 ± 0.0007	[7]
J1756-2251	1.312 ± 0.017	[7]
J1756-2251 c.	1.258 ± 0.017	[7]
J1807-2500B	1.3655 ± 0.0021	[7]
J1807-2500B c.	1.2064 ± 0.002	[7]
J1518+4904	$1.56 + 0.13 - 0.44$	[6]
J1518+4904 c.	$1.05 + 0.45 - 0.11$	[6]
J1811-1736	$1.56 + 0.24 - 0.45$	[6]
J1811-1736 c.	$1.12 + 0.47 - 0.13$	[6]
J1829+2456	$1.2 + 0.12 - 0.46$	[6]
J1829+2456 c.	$1.4 + 0.46 - 0.12$	[6]
GW170817 m_1	$\mathcal{P}(\mathcal{M}, q, z)$	[8]
GW170817 m_2	$\mathcal{P}(\mathcal{M}, q, z)$	[8]
GW190425 m_1'	$\mathcal{P}(m_1')$	[9]
GW190425 m_2'	$\mathcal{P}(m_2')$	[9]

TABLE II. Stars in NS-WD, all with mass measurements.

Star	Mass (in $M_\odot$)	Reference
J2045+3633	1.33 ± 0.3	[6, 7]
J2053+4650	1.4 ± 0.21	[6, 7]
J1713+0747	1.35 ± 0.07	[6, 7]
B1855+09	1.37 ± 0.13	[6, 7]
J0751+1807	1.72 ± 0.07	[6, 7]
J1141-6545	1.27 ± 0.01	[6, 7]
J1738+0333	1.47 ± 0.07	[6, 7]
J1614-2230	1.908 ± 0.016	[6, 7]
J0348+0432	2.01 ± 0.04	[6, 7]
J2222-0137	1.76 ± 0.06	[6, 7]
J2234+0611	1.393 ± 0.013	[6, 7]
J1949+3106	1.47 ± 0.43	[6, 7]
J1012+5307	1.83 ± 0.11	[6, 7]
J0437-4715	1.44 ± 0.07	[6, 7]
J1909-3744	1.48 ± 0.03	[6, 7]
J1802-2124	1.24 ± 0.11	[6, 7]
J1911-5958A	1.34 ± 0.08	[6, 7]
J2043+1711	1.38 ± 0.13	[6, 7]
J0337+1715	1.4378 ± 0.0013	[6, 7]
J1946+3417	1.828 ± 0.022	[6, 7]
J1918-0642	1.29 ± 0.1	[6, 7]
J1600-3053	2.3 ± 0.7	[6, 7]
J0621+1002	$1.7 + 0.1 - 0.17$	[6]
B2303+46	$1.38 + 0.06 - 0.1$	[6]
J0024-7204H	$1.48 + 0.03 - 0.06$	[6]
J0514-4002A	$1.49 + 0.04 - 0.27$	[6]
B1516+02B	2.1 ± 0.19	[6]
J1748-2446I	$1.91 + 0.02 - 0.1$	[6]
J1748-2446J	$1.79 + 0.02 - 0.1$	[6]
B1802-07	$1.26 + 0.08 - 0.17$	[6]
B1911-5958A	$1.4 + 0.16 - 0.10$	[6]
J0740+6620	$2.14 + 0.2 - 0.18$	[13]

A. NS Populations and Data

We study the NS populations based on the companion type of NS in binary systems. The companion star of a neutron star can be either another neutron star, or a white dwarf, or a main-sequence star. We refer to the NS-NS binaries as double neutron stars (or DNS), the NS – white dwarf as NS-WD, and the NS – main sequence as NS-MS. The main-sequence companion in an NS-MS binary can be either a low-mass or a high-mass X-ray binary (LMXB or HMXB). We only work with the population LMXB, which includes quiescent low-mass X-ray binaries (QLMXBs) and photospheric radius expansion X-ray bursts (PREs). In addition, we study the gravitational wave observations GW170817 and GW190425, both being treated as as DNS. Finally, we include the X-ray timing observations of two isolated pulsars by NICER – PSR J0030+0451 and PSR J0740+6620, which do not belong to either of the 3 populations.

We exclude the observations of binaries for which the masses were not measured, but otherwise constrained by the mass function, the total mass, or the mass ratio. Moreover, other populations not included in this work are the HMXBs, the binary black holes, and the NS – black hole (NS-BH) binaries.

The NS data types vary by their detection methods. Most stars in DNS (except GW170817 and GW190425), NS-WD, and some stars in LMXB have mass information with 68% uncertainties. We simply refer to this data set as "mass data". The electromagnetic data includes the rest of the stars in LMXBs (QLMXBs and PREs) and the NICER X-ray timing observations, which have 2-dimensional mass-radius probability distributions. The observation GW170817 has a 3-dimensional probability distribution of the chirp mass (in the detector frame), the mass ratio, and the redshift. The GW190425 data contains no information on redshift or tidal deformabilities. Therefore, we only use a 1-dimensional mass probability distributions for the two stars in GW190425.

The full list of stars included in our data sets is given in Tables I-III along with the references to their sources, which consists of 26 DNS, 32 NS-WD, and 15 LMXBs.

B. Parameters and Prior Choices

In order to perform Bayesian inference, we must specify the parameters and choose prior distributions for each.

TABLE III. Stars in LMXB, with mass data and mass-radius probability distributions (denoted as $\mathcal{P}$), except the two NICER stars at the bottom, which are isolated pulsars and do not belong to any population.

Star	Mass (in $M_\odot$)	Reference
Cyg X-2	1.71 ± 0.21	[7]
XTE J2123-058	1.53 ± 0.42	[7]
4U 1822-371	1.96 ± 0.36	[7]
Her X-1	1.073 ± 0.36	[7]
2S 0921-630	1.44 ± 0.1	[7]
47 Tuc (X7)	$\mathcal{P}(M,R)$	[10]
ω Cen		[10]
NGC 6304		[10]
NGC 6397		[10]
M13		[10]
M28		[10]
M30		[10]
SAX J1810.8-2609		[10]
4U 1702-429		[10]
4U 1724-307		[10]
PSR J0030+0451	$\mathcal{P}(M,R)$	[10]
PSR J0740+6620		[10]

1. Parameters

The parameters for the mass distribution model in Eq. (9) are the mean (μ) specifying the location, the standard deviation (σ) indicating the scale, and the skewness (α) of the distribution. Since each NS population has a different location, scale, and skewness, we have a mass distribution model for each population. Thus, we have 3 sets of parameters $(\mu_i, \sigma_i, \alpha_i)$ where $i = 1, 2, 3$ for the populations DNS, NS-WD, and LMXB.

The probability distribution given by Eq. (34) requires the NS masses to be free parameters. Hence, we have a total of 72 mass parameters (see Subsec. III A), which are denoted as $M_{i,j}$, where $i = 1, 2, 3$ for the 3 populations, and $j = 1, \ldots, N_i$, where N_i is the number of stars in the ith population.

The EoS parametrization involves 9 parameters. Starting from the low-density EoS in Eq. (15), the EoS parameters are the parameters a and α, the symmetry energy (S) and its derivative (L). Given S and L, we compute b and β using Eq. (16). At higher densities above $2n_0$, we use either the polytropic or the linear EoS. For the polytropic EoS, the parameters are $\gamma_1, E_1, \gamma_2, E_2, \gamma_3$; where γ_i are the exponents and E_k are the transition densities in Eq. (18) for each polytrope. As for the linear EoS, the exponents (γ_i) are replaced by the relative speeds of sound squared ($c^2_{s,i}$) for each line segment, while the transition densities (E_k) remain the same.

The gravitational observation GW170817 is described by the following parameters: the detector chirp mass ($\mathcal{M}_{\rm det}$), the mass ratio (q), and the redshift ($z_{\rm cdf}$). On the other hand, the GW190425 data contains no information about the tidal deformability as mentioned in Subsec. III A. Hence, the only parameter for GW190425 is the mass M_1.

See Table IV for the full list of parameters including their prior distributions.

2. Priors

As mentioned above, the likelihood is a function of 93 parameters along with the EoS parameters. For most of our parameters, we choose uniform distributions between the lower and upper limits given in Table IV:

TABLE IV. The index $i = 1, 2, 3$ for the NS populations; $j = 1, \ldots, N_i$, where N_i is the number of stars in the ith population; and $k = 1, 2$.

Parameter	Unit	Low	High
μ_i	$M_\odot$	0.5	2.5
$\log_{10}\sigma_i$		-6.0	0.0
α_i		-1.0	1.0
$M_{i,j}$	$M_\odot$	1.0	2.5
$m_{f,i}$		0.0	1.0
a	MeV	12.5	13.5
α		0.47	0.53
S	MeV	29.5	36.1
L	MeV	30.0	70.0
γ_i		10^{-6}	10.0
$c^2_{s,i}$		0.0	1.0
E_k	fm^{-4}	0.75	8.0
$\mathcal{M}_{\rm det}$	$M_\odot$	1.1917	1.1979
q		0.0	1.0
$z_{\rm cdf}$		0.0	1.0

All priors are uniform distributions except σ_i, which has a logarithmic distribution. Therefore, we choose $\log_{10}\sigma_i$ as the parameter so that it is uniform.

C. Inference of NS Mass Distribution

For clarity, we use the following indices to refer to the various populations: $i = 1$ for DNS, $i = 2$ for NS-WD, and $i = 3$ for LMXB. The number of stars in each population with mass measurements is N_1, N_2, and N_3. The number of stars in each population for which we have mass and radius (or tidal deformability) data is n_1, n_2, and n_3. Here, $n_1 = 4$ for the DNS in GW170817 and GW190425, $n_2 = 0$, and $n_3 = 10$.

We make the following definitions: $M_{i,j}$ is the neutron star mass (where j runs over all neutron stars in each of the three populations), $m_{i,j}$ is the mode of the neutron star mass measurement, $c_{i,j}$ and $d_{i,j}$ are the parameters describing the statistical uncertainty of the neutron star mass measurement, μ_i is the mode of the neutron star population, σ_i and α_i are parameters which describe the shape of the neutron star population, and $w_{i,j}$ is the systematic uncertainty in the neutron star measurements. As above, $w_{i,j} \equiv M_{i,j} - m_{i,j}$.

Thus, our parameters are $M_{i,j}$, μ_i, σ_i, α_i, and the EoS parameters $\{p\}$. The minimum neutron star mass is $M_{\rm min} \equiv 1\ {\rm M}_\odot$. The maximum neutron star mass, $M_{\rm max}$ is a function of the EoS parameters, i.e. $M_{\rm max} = M_{\rm max}(\{p\})$.

The combined likelihood function is

$$\begin{aligned}
&\mathcal{L}\left(\{\mu_i\},\{\sigma_i\},\{\alpha_i\},\{M_{i,j}\},\{p\}\right) = \\
&\prod_i^3 \prod_j^{N_i} \mathrm{AN}\left(w_{i,j},c_{i,j},d_{i,j}\right)\ \mathrm{SN}\left(\mu_i,\sigma_i,\alpha_i,M_{i,j}\right) \\
&\qquad \Theta\left(M_{\rm max}-M_{i,j}\right)\ \Theta\left(M_{i,j}-M_{\rm min}\right) \\
&\times \prod_j^4 \mathrm{SN}\left(\mu_1,\sigma_1,\alpha_1,M_{1,j}\right)\ \Theta\left(M_{\rm max}-M_{1,j}\right) \\
&\qquad \Theta\left(M_{1,j}-M_{\rm min}\right) \times \mathcal{L}_{\rm GW19}(m_1') \\
&\times \mathcal{L}_{\rm GW17}\Big[\mathcal{M}_{\rm det}(m_1,m_2,z), q(m_1,m_2), \tilde{\Lambda}(m_1,m_2,\{p\})\Big] \\
&\times \prod_j^{n_3} \mathrm{SN}\left(\mu_3,\sigma_3,\alpha_3,M_{3,j}\right)\ \mathcal{D}\left[R(M_{3,j},\{p\}),\ M_{3,j}\right] \\
&\qquad \Theta\left(M_{\rm max}-M_{3,j}\right)\ \Theta\left(M_{3,j}-M_{\rm min}\right) \qquad (34)
\end{aligned}$$

D. Changing parameters

We want to see how the results change when we make the maximum mass a parameter with a flat prior distribution. To do this, we make a variable transformation. Before the transformation, the likelihood is of the form $\mathcal{L}(\ldots,\{p\})$ given above in Eq. (34) and the prior (which we assume to be a product of independent factors) is

$$\prod_i P(\mu_i)P(\sigma_i)P(\alpha_i)\prod_{i,j}P(M_{i,j})\prod_k P(p_k)\,, \qquad (35)$$

where i is 1, 2, or 3, j runs over all the neutron stars in each class, and k indexes the EoS parameters. Our goal is to modify the prior distribution to the new form

$$\prod_i P(\mu_i)P(\sigma_i)P(\alpha_i)\prod_{i,j}P(M_{i,j})\prod_{k=1}^{N_k-1} P(p_k)P(M_{\rm max})\,, \qquad (36)$$

which we can do with the identity

$$P(M_{\rm max}) = \frac{\partial p_N}{\partial M_{\rm max}} P(p_{N_k})\,. \qquad (37)$$

Thus, the new likelihood is

$$\mathcal{L}(\ldots,p_1,p_2,\ldots,p_{N_k-1},M_{\rm max}) = \mathcal{L}(\ldots,\{p\})\frac{\partial p_N}{\partial M_{\rm max}}\,. \qquad (38)$$

We apply this change of parameters to both EoS models NL (linear) and NP (polytropic), and refer to the variant models by ML and MP, respectively.

IV. RESULTS AND DISCUSSION

In this section, we present the current results for the EoS and the mass distribution models. Then we provide an overview of recent works and compare our results. Note that this work is still in progress while we wait for our MCMC simulations to reach equilibrium, and that the final results may change to some extent.

A. Results

For reference, models NL and NP refer to the linear and the polytropic EoS, respectively. Models ML and MP are the variants of NL and NP, respectively, where the likelihood is a function of the maximum mass, in addition to the other parameters.

The equations of state are given in Fig. 1. The polytropic EoS models (NP and MP) are relatively stiff, that is, the pressure increases more rapidly with increasing density, and therefore, provide more support against gravitational compression. The linear EoS models (NL and ML) are soft, but more constrained compared to the polytropic models. Note that the uncertainties in all equations of state increase with the density, particularly above $\epsilon = 700-750$ MeV fm^{-3}. However, the model ML is significantly well constrained even at the highest densities, which is a distinct feature of this model. As expected, all equations of state are continuous, but the linear models NL and ML have sharp transitions at some densities between $290-320$ MeV fm^{-3}, where the derivatives $dP/d\epsilon = c_s^2$ are discontinuous. Since these models assume a fixed speed of sound in each line segment separated by the transition densities, such sudden changes in c_s may indicate phase transitions at these densities.

Fig. 2 shows the corresponding mass-radius curves for the EoS models. As seen in the figure, the $M-R$ curves for the linear models NL and ML have less uncertainties, reflecting their corresponding well-constrained equations of state. However, these linear models also lead to smaller radii for neutron stars with masses between $0.5-1.0\ M_\odot$. The widths and the tails of the curves indicate that the radii are better constrained for NS masses above $0.5\ M_\odot$ and becomes highly uncertain for smaller masses. In particular, the stars with the most constrained radii have masses between $1.4-1.6\ M_\odot$. The peak in each curve represent the stars with the maximum mass, which have smaller radii ($\approx 11.8-12.2$ km) reflecting the compactness of neutron stars.

The posteriors for the maximum mass supported by each model are given in Fig. 3. The sharp cutoff at $M_{\rm max} = 2.0\ M_\odot$ reflects our imposed constraint on the lower bound that $M_{\rm max} \geq 2.0\ M_\odot$. Note that the probability densities are highly skewed toward smaller maximum masses, and this skewness is independent of the cutoff at $2\ M_\odot$. The model ML accommodate the most massive stars with the peak centered at $M_{\rm max} = 2.14\ M_\odot$ and has wider support (up to $\approx 2.56\ M_\odot$). On the other

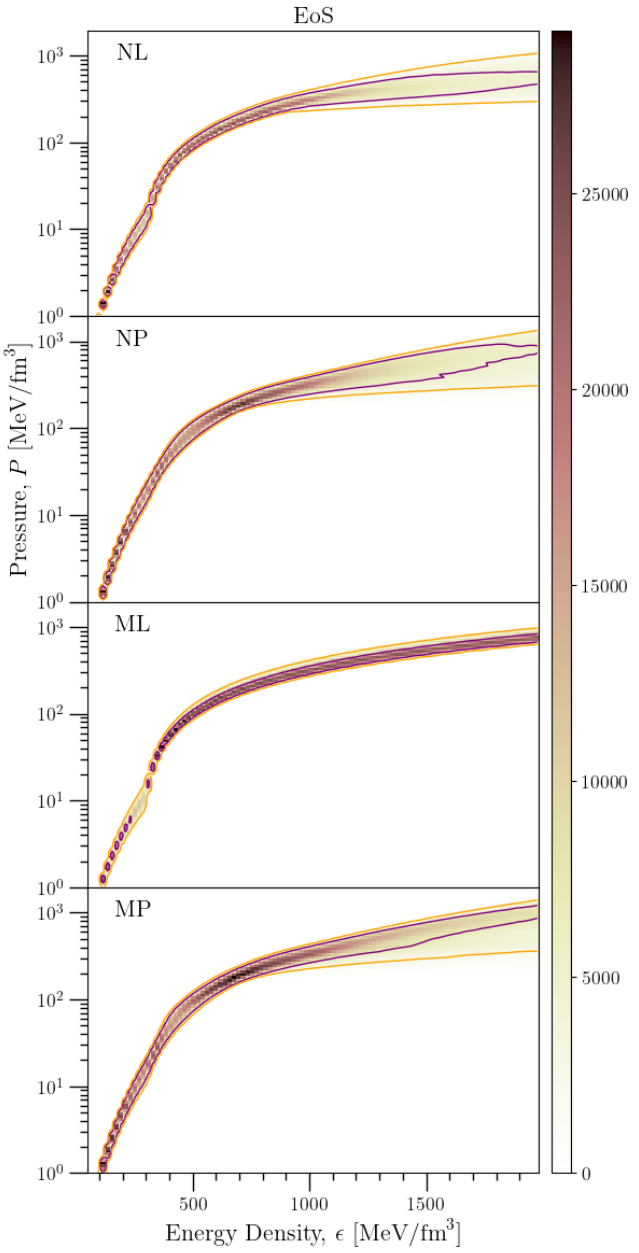

FIG. 1. EoS models with 68% (purple) and 95% (orange) confidence levels. The color map shows number of points. Models NL and NP are linear and polytropic, respectively. ML and MP are the variants of NL and MP, respectively, where the likelihood is also a function of $M_{\max}$. NL and ML are soft, NP and MP are relatively stiff, which shows that stiffness in EoS results from prior choice. The model ML is highly constrained at all densities.

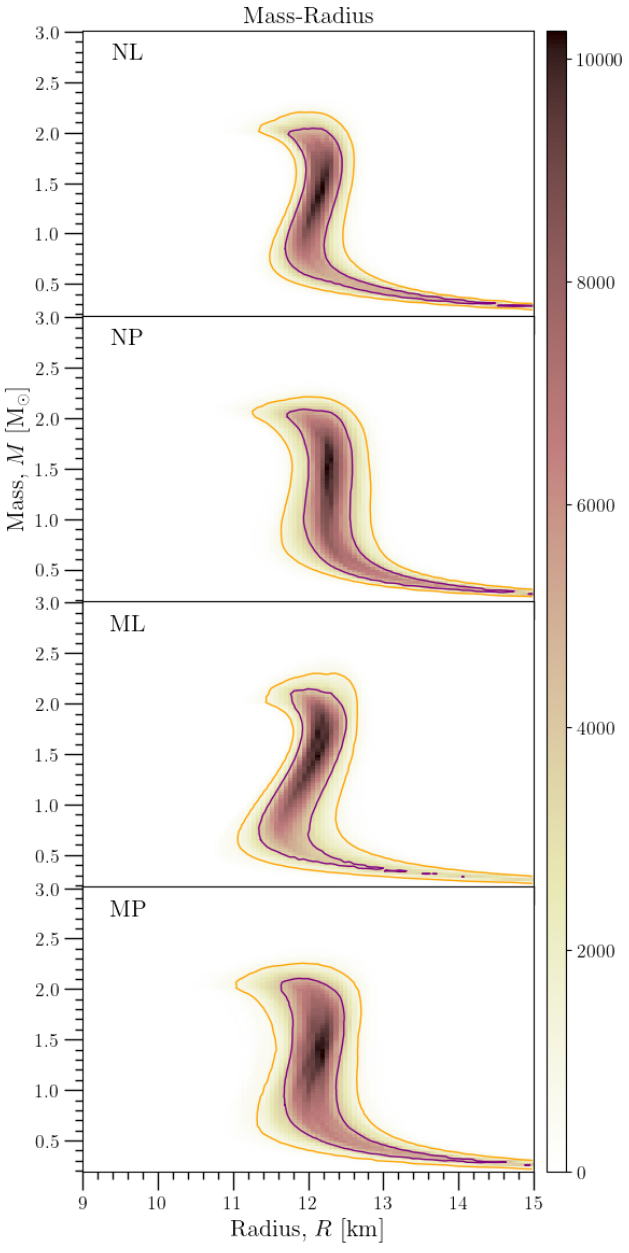

FIG. 2. $M - R$ curves for the corresponding EoS in Fig. 1, with 68% (purple) and 95% (orange) confidence levels. The color map shows number of points. The radii are better constrained for NS with masses between $1.4 - 1.6\ M_\odot$, but becomes highly uncertain for below $0.5\ M_\odot$. The peaks represent the most massive stars with smaller radii, reflecting compactness of neutron stars.

hand, the model NL has the narrowest density with the peak at $M_{\max} = 2.08\ M_\odot$. Thus, the linear EoS models represent the two extreme cases in regards to the NS maximum mass, while the polytropic models NP and MP fall in between with peaks at 2.1 $M_\odot$ and 2.12 $M_\odot$, respectively.

Fig. 4 shows the posterior mass distributions of the populations grouped by the EoS models. The rows represent different EoS models and the columns show different population types. As seen in the figure, the peaks of the probability densities do not deviate significantly for different EoS models, because their only connection to the EoS models is through the maximum mass (and

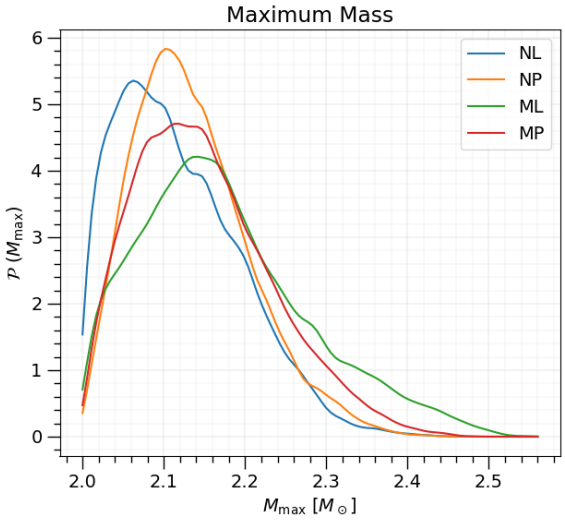

FIG. 3. The probability densities of the NS maximum mass, with skewness toward lower $M_{\rm max}$, which is independent of the cutoff at 2.0 $M_\odot$. The linear EoS models exhibits the extreme cases: ML has the widest support for higher $M_{\rm max}$ with the peak at 2.14 $M_\odot$, while NL is the narrowest with the peak at 2.08 $M_\odot$, which is barely above the cutoff.

the total log-likelihood), which is a function of the EoS parameters. However, the densities vary in widths and skewness for different EoS models. Particularly, the distributions of LMXB exhibit a stronger dependence on the prior choices of the EoS (and the maximum mass). This is because most stars in LMXB have mass-radius observations (see Table III), as opposed to direct mass measurements, which are correlated to the EoS priors.

The peaks of the densities for DNS, NS-WD, and LMXB are located around 1.4 $M_\odot$, 1.6 $M_\odot$, and 1.7 $M_\odot$, respectively. The stars in DNS have relatively well-measured masses, and therefore, have the narrowest distributions with an average width 0.17 $M_\odot$. On the other hand, NS-WD contains massive stars (above 2 $M_\odot$) and has larger uncertainties in mass measurements, which result into wider distributions (width 0.24 $M_\odot$). The LMXBs also consist of relatively massive neutron stars due to mass accretion from their low-mass companions (width 0.19 $M_\odot$). Finally, we observe nearly zero skewness for the distributions DNS and NS-WD, but LMXB has an overall negative (left) skewness.

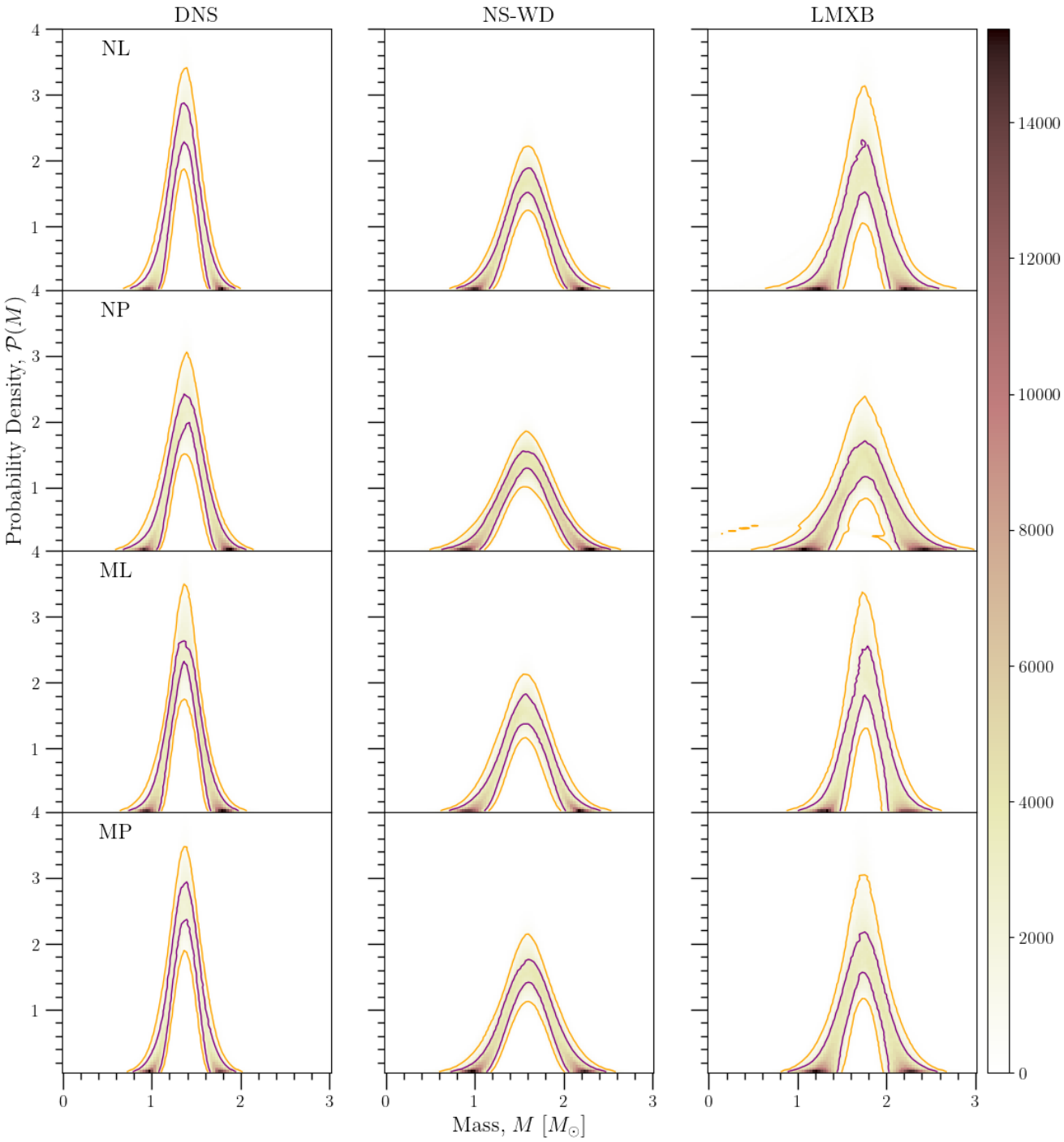

FIG. 4. The mass distributions of NS populations, grouped by the EoS models, with contour lines representing 68% (purple) and 95% (orange) confidence levels. The probability densities for each population are normalized (contour lines are un-normalized) and slightly vary by EoS models. The peaks for DNS, NS-WD, and LMXB are centered at 1.4 ± 0.17 $M_\odot$, 1.6 ± 0.24 $M_\odot$, and 1.7 ± 0.19 $M_\odot$, respectively. Row-wise plots represent the same EoS model for different populations. The color map shows number of points.

B. Discussion

Bayesian analysis has become a natural choice and a powerful tool in modeling NS mass distributions, and studying EoS models and mass-radius relations since the last decade [14–16]. As explained in Section III, Bayesian inference requires specifying a statistical model for each observable under study with a number of model parameters (and/or hyperparameters). Thus, previous studies have used various statistical models of NS mass distributions (in binaries) for different types of data. While some works primarily focused on single-model distributions based on the measured observables and the evolution stages, or the population types [5–7], most works considered either weighted bi-model distributions or a combination of both (multi-model) using the Bayes factor or hyperparameters for model selection [17–21]. For example, the data types with different measured observables in these studies include constraints on either the NS mass, the mass function, the total mass, or the mass ratio. The most commonly used mass distributions in these works include power laws for the mass ratios and the NS-BH binaries, uniform, single-component Gaussian (normal) distributions, and weighted multi-component Gaussian mixture models for the NS masses.

Our assumption that different NS populations have different mass distributions and that each population can be described by a fixed distribution, requires us to consider only single-model distributions. Moreover, our NS mass data contains asymmetries in the uncertainties of mass measurements, particularly the DNS and the NS-WD binaries. Therefore, we adopt the statistical model from Kiziltan *et al.* [6] which introduces skewness as an extension to a simple normal distribution, instead of two- or multi-component Gaussian distributions. Thus, this model accommodates our assumptions as well as the asymmetries in mass uncertainties. However, our model is distinct from Ref. [6] where the likelihood is only a function of model parameters and marginalized over all NS masses. On the other hand, we compute the likelihood for each star as a function of the individual NS masses, in addition to the model parameters. This technique allows us to use the NS masses as free parameters and combine our mass distribution model with the one from Ref. [10].

As for the NS maximum mass, most works simply used $M_{\rm max}$ as a free parameter and imposed a zero likelihood of mass $M > M_{\rm max}$, while some focused on constraining $M_{\rm max}$ based on galactic NS observations [19] in addition to predictions from dense matter EoS models [21]. The latter approach is our natural choice since we compute $M_{\rm max}$ directly from the TOV equation, which is an advantage in combining mass distributions with EoS models. However, instead of using $M_{\rm max}$ as a free parameter, we make a change of variable (see Subsec. II B) so that our likelihood is also a function of $M_{\rm max}$ with a uniform prior distribution. This technique simultaneously allows us to avoid using an additional parameter and study how different assumptions on $M_{\rm max}$ impact the EoS at the highest densities.

V. FUTURE WORK

Our EoS models contain no information regarding nuclear interactions at baryon densities above $2n_0$. While the dense matter EoS is well constrained with microscopic calculations of 2- and 3-nucleon interactions based on chiral effective field theory (EFT), constraining EoS at higher densities heavily rely on macroscopic astrophysical observations. To fully understand the structure and composition of neutron star cores, and more generally, the nature of dense matter, knowledge of microscopic interactions at high densities is crucial.

Focused on the aspect mentioned above, some recent works include constraining the low-density EoS using chiral EFT to next-to-next-to-next-to leading order (N3LO) and many-body corrections up to 3-nucleons [22], studying the existence of quark matter and comparing with observational data [23], and connecting the theoretical constraints on the low-density EoS with terrestrial experiments and astrophysical observations at higher densities [24]. On the other hand, Ref. [25] presented another approach to constraining the dense matter EoS by using a population synthesis model, which included the DNS population from Ref. [7] as in our work. However, this study did not include radius constraints from EM observations, nor did it consider a realistic EoS model.

In our future work, we aim to incorporate hadronic interactions into our dense matter EoS models involving nucleons, pions, and hyperons. In addition, we also plan to include constraints from the GW170817 kilonova and r-process nucleosynthesis from Ref. [25].

My plan is to submit my first first-author paper by the end of the calendar year, and my second first-author paper by the end of 2024. My Ph.D. thesis will involve these two projects, with which I plan to graduate by the summer of 2025.

ACKNOWLEDGEMENT

We thank Satyajit Roy, Sanket Sharma, Zidu Lin, and Richard O'Shaughnessy for their useful insights and helps with producing the plots, developing the code, and for raising thoughtful questions. This project is supported by the National Science Foundation grant AST 22-06322, in collaboration with Richard O'Shaughnessy.

Appendix A: Skewed and Asymmetric Normal Distributions

The probability distribution function ϕ and the cumulative distribution function Φ of the normal distribution $N(\mu,\sigma)$ in Eq. (9) are given by

$$\phi\left(\frac{x-\mu}{\sigma}\right) = \frac{1}{\sqrt{2\pi}}\exp\left[-\frac{1}{2}\left(\frac{x-\mu}{\sigma}\right)^2\right]$$
$$\Phi\left(\frac{x-\mu}{\sigma}\right) = \frac{1}{2}\left[1+\mathrm{erf}\left(\frac{x-\mu}{\sigma\sqrt{2}}\right)\right],$$

where, the error function is

$$\mathrm{erf}(x) = \frac{2}{\sqrt{\pi}}\int_0^x e^{-t^2}dt. \tag{A1}$$

Then the skewed normal distribution function in in Eq. (9) can be written as

$$\mathrm{SN}(M\,|\,\mu,\sigma,\alpha) = \frac{1}{\sigma\sqrt{2\pi}}\exp\left[-\frac{1}{2}\left(\frac{M-\mu}{\sigma}\right)^2\right] \times\left[1+\mathrm{erf}\left[\frac{(M-\mu)\alpha}{\sigma\sqrt{2}}\right]\right]$$

The asymmetric normal distribution function with parameters $c,d>0$ given by Eq. (10) is:

$$\mathrm{AN}(x\,|\,c,d) = \frac{2}{d\,(c+1/c)}\left[\phi\left(\frac{x}{cd}\right)\chi_{[0,\infty)}(x) + \phi\left(\frac{cx}{d}\right)\chi_{(-\infty,0)}(x)\right]$$
$$= \begin{cases} \dfrac{2}{d\,(c+1/c)}\dfrac{1}{\sqrt{2\pi}}\exp\left[-\dfrac{1}{2}\left(\dfrac{cx}{d}\right)^2\right] & \text{if } x<0 \\ \dfrac{2}{d\,(c+1/c)}\dfrac{1}{\sqrt{2\pi}}\exp\left[-\dfrac{1}{2}\left(\dfrac{x}{cd}\right)^2\right] & \text{if } x\geq 0, \end{cases}$$

where ϕ is the density function of the standard normal distribution $N(0,1)$ and $\chi_A(\cdot)$ is the indicator function of set A.

Appendix B: Calculation of Parameters (c, d)

Here we show how the parameters $c_{i,j}$, $d_{i,j}$ for the jth star in the ith population are calculated. Here we suppress the notations i,j for simplicity.

The calculation of the parameter c is straightforward. Let l and u be the 68% lower and upper limits of the NS mass, respectively. The condition

$$\mathrm{AN}(-l\,|\,c,d) = \mathrm{AN}(u\,|\,c,d),$$

implies that

$$\phi\left(-\frac{cl}{d}\right) = \phi\left(\frac{u}{cd}\right)$$
$$\implies \exp\left[-\frac{1}{2}\left(-\frac{cl}{d}\right)^2\right] = \exp\left[-\frac{1}{2}\left(\frac{u}{cd}\right)^2\right]$$
$$\implies \frac{cl}{d} = \frac{u}{cd}.$$

Thus we have

$$c = \sqrt{\frac{u}{l}} \tag{B1}$$

Given c by Eq. (B1), now we want to solve for the parameter d such that

$$\int_{-l}^{u}\mathrm{AN}(x\,|\,c,d)\,dx = 0.68, \tag{B2}$$

where the parameter $c\equiv\sqrt{u/l}$. Note that the error function and its first-order derivative (with and without a scale parameter a) are, respectively,

$$\mathrm{erf}(x) = \frac{2}{\sqrt{\pi}}\int_0^x e^{-t^2}\,dt; \quad \frac{d}{dx}\mathrm{erf}(x) = \frac{2}{\sqrt{\pi}}e^{-x^2};$$
$$\frac{d}{dx}\mathrm{erf}(ax) = \frac{2a}{\sqrt{\pi}}e^{-(ax)^2}.$$

The last result can be multiplied by a factor to obtain:

$$\frac{1}{d\big(c+1/c\big)}\frac{1}{a\sqrt{2}}\frac{d}{dx}\mathrm{erf}(ax) = \mathrm{AN}(x\,|\,c,d). \tag{B3}$$

Here, the parameter a is defined as:

$$a = \begin{cases} \dfrac{c}{\sqrt{2}d} = a_< & \text{if } x<0, \\ \dfrac{1}{\sqrt{2}cd} = a_> & \text{if } x\geq 0. \end{cases}$$

Substituting Eq. (B3) into (B2):

$$\frac{1}{\sqrt{2}a_<d(c+1/c)}\int_{-l}^{0}dx\,\frac{d}{dx}\mathrm{erf}(a_<x) + \frac{1}{\sqrt{2}a_>d(c+1/c)}\int_0^u dx\,\frac{d}{dx}\mathrm{erf}(a_>x) = 0.68$$

$$\implies \frac{1}{c^2+1}\left[-\mathrm{erf}(a_<x)|_{-l}\right] + \frac{1}{1+1/c^2}\left[\mathrm{erf}(a_>x)|_u\right] = 0.68$$
$$\implies c^2\,\mathrm{erf}(a_>u) - \mathrm{erf}(-a_<l) = 0.68(c^2+1)$$
$$\implies c^2\,\mathrm{erf}\left(\frac{u}{\sqrt{2}cd}\right) - \mathrm{erf}\left(-\frac{cl}{\sqrt{2}d}\right) - 0.68\left(c^2+1\right) = 0 \tag{B4}$$

Given the asymmetry parameter c, Eq. (B4) can be used to solve for the scale parameter d.

Appendix C: Bayesian Inference

For some observation (or data) d, model parameter θ, and prior distribution $\mathcal{P}(\theta)$, Bayes's theorem states that the posterior distribution of d given θ is

$$\mathcal{P}(\theta|d) = \frac{\mathcal{P}(d|\theta)\,\mathcal{P}(\theta)}{\mathcal{P}(d)}, \tag{C1}$$

where $\mathcal{P}(d|\theta)$ is the likelihood of the observations d given the parameters θ, and $\mathcal{P}(d)$ is the normalization constant defined as:

$$\mathcal{P}(d) = \int \mathcal{P}(d|\theta)\ \mathcal{P}(\theta)\ d\theta, \tag{C2}$$

which is marginalized over all parameters θ, and so, is called the prior predictive distribution. The product

$$\mathcal{P}(d, \theta) = \mathcal{P}(d|\theta)\ \mathcal{P}(\theta)$$

is often called a joint distribution.

For a new observation m, given the previous observation d, the integral

$$\mathcal{P}(m|d) = \int \mathcal{P}(m|d, \theta)\ \mathcal{P}(\theta|d)\ d\theta,$$

gives the posterior predictive distribution of m. If the observations m and d are independent of each other, then the integrand in the above expression simplifies to

$$\mathcal{P}(m|d) = \int \mathcal{P}(m|\theta)\ \mathcal{P}(\theta|d)\ d\theta. \tag{C3}$$

[1] A. W. Steiner, C. O. Heinke, S. Bogdanov, C. K. Li, W. C. G. Ho, A. Bahramian, and S. Han, Monthly Notices of the Royal Astronomical Society **476**, 421 (2018).
[2] J. Nättilä, V. F. Suleimanov, J. J. E. Kajava, and J. Poutanen, A&A **581**, A83 (2015).
[3] T. E. Riley, A. L. Watts, S. Bogdanov, P. S. Ray, R. M. Ludlam, S. Guillot, Z. Arzoumanian, C. L. Baker, A. V. Bilous, D. Chakrabarty, *et al.*, The Astrophysical Journal Letters **887**, L21 (2019).
[4] M. C. Miller, F. K. Lamb, A. J. Dittmann, S. Bogdanov, Z. Arzoumanian, K. C. Gendreau, S. Guillot, W. C. G. Ho, J. M. Lattimer, M. Loewenstein, *et al.*, The Astrophysical Journal Letters **918**, L28 (2021).
[5] F. Özel, D. Psaltis, R. Narayan, and A. S. Villarreal, The Astrophysical Journal **757**, 55 (2012).
[6] B. Kiziltan, A. Kottas, M. D. Yoreo, and S. E. Thorsett, The Astrophysical Journal **778**, 66 (2013).
[7] J. Alsing, H. O. Silva, and E. Berti, Monthly Notices of the Royal Astronomical Society **478**, 1377 (2018).
[8] B. P. Abbott *et al.* (LIGO Scientific Collaboration and Virgo Collaboration), Phys. Rev. Lett. **119**, 161101 (2017).
[9] B. P. Abbott *et al.* (LIGO Scientific Collaboration and Virgo Collaboration), The Astrophysical Journal Letters **892**, L3 (2020).
[10] M. Al-Mamun, A. W. Steiner, J. Nättilä, J. Lange, R. O'Shaughnessy, I. Tews, S. Gandolfi, C. Heinke, and S. Han, Phys. Rev. Lett. **126**, 061101 (2021).
[11] S. Gandolfi, J. Carlson, and S. Reddy, Phys. Rev. C **85**, 032801 (2012).
[12] A. W. Steiner, S. Gandolfi, F. J. Fattoyev, and W. G. Newton, Phys. Rev. C **91**, 015804 (2015).
[13] H. T. Cromartie, E. Fonseca, S. M. Ransom, P. B. Demorest, Z. Arzoumanian, H. Blumer, P. R. Brook, M. E. DeCesar, T. Dolch, J. A. Ellis, *et al.*, Nature Astronomy **4**, 72 (2020).
[14] A. W. Steiner, J. M. Lattimer, and E. F. Brown, The Astrophysical Journal **722**, 33 (2010).
[15] F. Özel, G. Baym, and T. Güver, Phys. Rev. D **82**, 101301 (2010).
[16] B. Kiziltan, A. Kottas, and S. E. Thorsett, (2010), arXiv:1011.4291 [astro-ph.GA].
[17] J. Antoniadis, T. M. Tauris, F. Ozel, E. Barr, D. J. Champion, and P. C. C. Freire, (2016), arXiv:1605.01665 [astro-ph.HE].
[18] N. Farrow, X.-J. Zhu, and E. Thrane, The Astrophysical Journal **876**, 18 (2019).
[19] K. Chatziioannou and W. M. Farr, Phys. Rev. D **102**, 064063 (2020).
[20] M. Fishbach, R. Essick, and D. E. Holz, The Astrophysical Journal Letters **899**, L8 (2020).
[21] P. Landry and J. S. Read, The Astrophysical Journal Letters **921**, L25 (2021).
[22] J. Keller, K. Hebeler, and A. Schwenk, Phys. Rev. Lett. **130**, 072701 (2023).
[23] P. T. H. Pang, L. Sivertsen, R. Somasundaram, T. Dietrich, S. Sen, I. Tews, M. Coughlin, and C. V. D. Broeck, (2023), arXiv:2308.15067 [nucl-th].
[24] S. Huth, P. T. H. Pang, I. Tews, T. Dietrich, A. L. Fèvre, A. Schwenk, W. Trautmann, K. Agarwal, M. Bulla, M. W. Coughlin, and C. V. D. Broeck, Nature **606**, 276 (2022).
[25] E. M. Holmbeck, R. O'Shaughnessy, V. Delfavero, and K. Belczynski, The Astrophysical Journal **926**, 196 (2022).